Mono- and ditopic hydroxamate ligands towards discrete and extended network architectures

Fugu, Mohammed B.; Ellaby, Rebecca J.; O`Connor, Helen M.; Pitak, Mateusz B.; Klooster , Wim ; Horton, Peter N.; Coles, Simon J.; Al-mashhadani, Mohammed H.; Brechin, Euan K.; Perepichka, Igor; Jones, Leigh F.

Dalton Transactions

DOI:
10.1039/C9DT01531K

Published: 01/07/2019

Peer reviewed version

Mono- and ditopic hydroxamate ligands towards discrete and extended network architectures

Mohammed B. Fugu,[a] Rebecca J. Ellaby,[a] Helen M. O'Connor,[b] Mateusz B. Pitak,[c] Wim Klooster,[c] Peter N. Horton,[c] Simon J. Coles,[c] Mohammed H. Al-mashhadani,[a,d] Igor F. Perepichka,[e] Euan K. Brechin[b] and Leigh F. Jones.*[a]

[a] *School of Natural Sciences, Bangor University, Bangor, Wales, LL57 2DG, UK. Tel: +44(0)1248-38-2391. Email: leigh.jones@bangor.ac.uk.*

[b] *EaStCHEM School of Chemistry, David Brewster Road, University of Edinburgh, Edinburgh, Scotland, EH9 3FJ, UK.*

[c] *UK National Crystallographic Service, Chemistry, Faculty of Natural and Environmental Sciences, University of Southampton, England, UK. SO17 1BJ.*

[d] *Chemistry Department, College of Science, Al-Nahrain University, Baghdad, Iraq*

[e] *Shaanxi Institute of Flexible Electronics, Northwestern Polytechnical University, 127 West Youyi Road, Xi'an 710072, Shaanxi, China*

Abstract

A family of mono- and ditopic hydroxamic acids have been employed in the synthesis, structural and physical characterisation of discrete (0D) and (1- and 2-D) extended network coordination complexes. Examples of the latter include the 1-D coordination polymer $\{[Zn(II)(L_3H)_2]\cdot 2MeOH\}_n$ (**5**; L_3H_2 = 2-(methylamino)phenylhydroxamic acid) and the 2-D extended network $\{[Cu(II)(L_2H)(H_2O)(NO_3)]\cdot H_2O\}_n$ (**4**; L_2H_2 = 4-amino-2-(acetoxy)phenylhydroxamic acid). The 12-MC-4 metallacrown $[Cu(II)_5(L_4H)_4(MeOH)_2(NO_3)_2]\cdot 3H_2O.4MeOH$ (**7**) represents the first metal complex constructed using the novel ligand N-hydroxy-2-[(2-hydroxy-3-methoxybenzyl)amino]benzamide (L_4H_3). Variable temperature magnetic susceptibility studies confirm strong antiferromagnetic exchange between the Cu(II) centres in **7**. Coordination polymer **5** shows photoluminescence in the blue region (λ_{PL} ~ 421 – 450 nm) with a bathochromic shift of the emission (~ 15 – 30 nm) from solution to the solid state.

Introduction

The O,O´-bidentate chelating ability of the hydroxamate functional group towards a range of transition metals engenders hydroxamic acids as excellent ligands / bioactive agents in the fields of coordination chemistry, bioinorganic chemistry, chemical biology and medicine. Such

properties afford these organic acids rich toxicological, pharmacological and pathological bioactivities, leading to their prominence as selective enzyme inhibitors[1] and as vital elements in a variety of therapeutic drugs.[1-2]

More specifically, the exceptionally strong binding affinities of hydroxamic acids towards Fe(III) ions in solution[3] is best exampled through their integral roles as iron chelators in the treatment of iron overload therapy[4] and as prominent building blocks within iron scavenging sidephore architectures.[1c,5] Moreover, hydroxamic acids have been extensively employed in the metal extraction and recovery of a number of transition metals,[6] and have shown an inherent ability to coordinate to a plethora of transition metal ions in the crystalline solid state.[1c] Although the O,O´-bidentate chelating binding mode is regularly observed in crystal structures of metal complexes and metalloproteins alike, more recent investigations into the coordination chemistry of hydroxamic acids tend to focus on the behaviour of their polyfunctional analogues that are employed to transcribe a diverse range of binding modes upon more elaborate polymetallic architectures such as those of the homo- and heterometallic metallacrowns.[7]

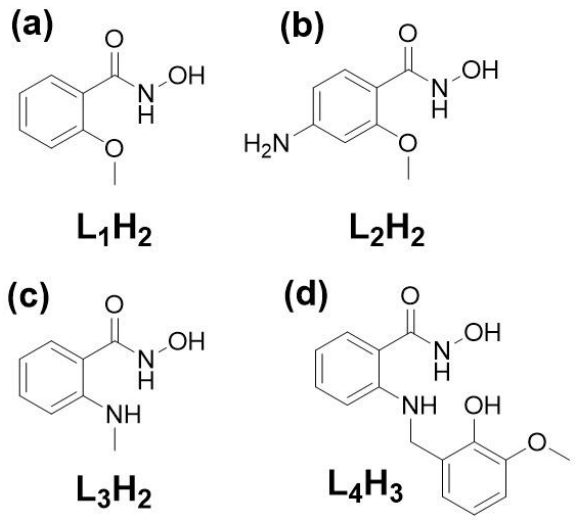

Scheme 1 ChemDraw representations of the ligands 2-(acetoxy)phenyl hydroxamic acid (L_1H_2; a), 4-amino-2-(acetoxy)phenylhydroxamic acid (L_2H_2; b), 2-(methylamino)phenylhydroxamic acid (L_3H_2; c) and *N*-hydroxy-2-((2-hydroxy-3-methoxybenzyl)amino)benzamide (L_4H_3, d).

Our previous investigations into the coordination chemistry of the ligands 2-(dimethylamino)phenylhydroxamic acid (2-dma-phaH_2) and 2-(amino)phenylhydroxamic acid (2-am-phaH_2) initially led to the formation of a family of planar 12-MC-4 [M(II)] (M = Ni, Cu)

metallacrowns, which included the complexes: $[Cu(II)_5(2\text{-dma-pha})_4(MeOH)_4](ClO_4)_2$, $[Ni(II)_5(2\text{-dma-pha})_4(MeOH)_4](ClO_4)_2 \cdot 2MeOH$[8] and $[Cu(II)_5(2\text{-am-pha})_4(MeOH)_4](ClO_4)_2 \cdot H_2O$,[9] The apparent stability of these pentametallic metallacrown architectures was further highlighted upon successful employment as nodes in the construction of the 1- and 2-D coordination polymers: $\{[Cu(II)_5(2\text{-dma-pha})_4(4,4\text{-bipy})_3](ClO_4)_2 \cdot (H_2O)\}_n$ (4,4-bipy = 4,4-bipyridyl), $\{[Cu(II)_5(2\text{-dma-pha})_4(4,4\text{-azp})_2(MeOH)_2](ClO_4)_2\}_n$ and $\{[Cu(II)_5(2\text{-am-pha})_4(pz)_2(MeOH)_3](ClO_4)_2 \cdot MeOH\}_n$ (4,4-azp = 4,4-azopyridine; pz = pyrazine).[9]

Results and Discussion

Herein we describe the synthesis of the ligands 2-(acetoxy)phenylhydroxamic acid (L_1H_2), 4-amino-2-(acetoxy)phenyl hydroxamic acid (L_2H_2), 2-(methylamino)phenylhydroxamic acid (L_3H_2) and *N*-hydroxy-2-[(2-hydroxy-3-methoxybenzyl)amino)]benzamide (L_4H_3) (Scheme 1) along with their employment in the formation of numerous discrete mono- and polymetallic cages and coordination polymers. More specifically, we present the first examples of 3d transition metal complexation of these ligands in the form of (for instance) the complexes $[Cu(II)(L_1H)_2]$ (**1**), $[Fe(III)_2(L_1H)_4Cl_2] \cdot 2MeCN$ (**2**) and $[Co(III)Co(II)_6(L_1H)_8(L_1)_2(MeOH)_4(NO_3)_2]NO_3 \cdot 3.5H_2O \cdot 14MeOH$ (**3**) as well as the pentametallic 12-MC-$4_{Cu(II)}$ metallacrowns $[Cu(II)_5(L_2)_4(NO_3)_2] \cdot 3H_2O$ (**6**) and $[Cu(II)_5(L_4H)_4(MeOH)_2(NO_3)_2] \cdot 3H_2O \cdot 4MeOH$ (**7**). We also present the coordination polymers $\{[Zn(II)(L_3H)_2]_n \cdot 2MeOH\}_n$ (**5**) (1D chain) and $\{[Cu(II)(L_2H)(H_2O)(NO_3)] \cdot H_2O\}_n$ (**4**) (2D [4,4] net). Crystallographic information for complexes **1**-**7** are given in Tables S1 and S2 (electronic supplementary information).

We began by investigating the coordination chemistry of the ligand 2-(acetoxy)phenyl hydroxamic acid (L_1H_2). Reaction of $Cu(NO_3)_2 \cdot 3H_2O$, L_1H_2 and NaOH in MeOH gave rise to a dark green mother liquor from which needle shaped crystals of $[Cu(II)(L_1H)_2]$ (**1**) were obtained. Complex **1** crystallises in the monoclinic $P2_1/c$ space group. The structure in $[Cu(II)(L_1H)_2]$ (**1**) comprises a single square planar Cu(II) ion (O1-Cu1-O1 = 180°) connected to two singly deprotonated L_1H^- ligands, each utilising a chelating coordination mode and giving rise to Cu-O bond lengths of 1.94 Å (Cu1-O1) and 1.91 Å (Cu1-O2) (Fig. 1). As illustrated in Figure 1(a), a centre of inversion lies at the metal centre. Both of the hydroxamate ligands in **1** remain protonated at the amide N atom (N1-H1) and are therefore able to partake in intramolecular H-bonds with their neighbouring OCH_3 groups as shown by the dashed lines in Figure 1(b) (N1(H1)···O3 = 2.00 Å). The individual $\{Cu_1\}$ units in **1** align into

superimposable stacks along the *a*-direction of the unit cell (Cu1···Cu1' = 3.70 Å) and these individual rows are arranged in an efficient brickwork pattern along the *bc* cell plane (Fig. S1). This packing arrangement is supported by numerous intermolecular H-bonding interactions (*e.g.* C6(H6)···O2' = 2.40 Å, C8(H8A)···O2' = 2.48 Å and C5(H5)···O3 = 2.60 Å).

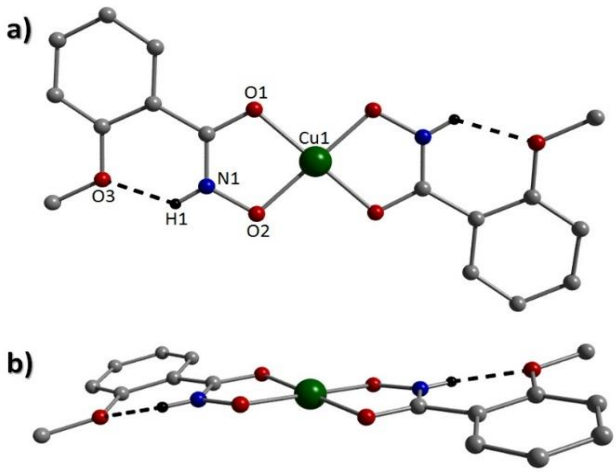

Figure 1 Structure of **1** as viewed perpendicular (a) and parallel (b) to the {Cu(II)O_4} plane. Black dashed lines represent intramolecular hydrogen bonding (N1(H1)···O3 = 1.98 Å). Colour code (as used throughout the manuscript): Green (Cu), Red (O), Blue (N), grey (C) and black (H). The majority of hydrogen atoms have been omitted for clarity.

Using a Johnson Matthey balance, the room temperature magnetic moment (μ_{eff}) of **1** (1.61 BM) was found to be consistent with that expected for a monometallic square planar Cu(II) complex ($\mu_{S.O.}$ = 1.73 BM) (Table S3). Complex **1**, along with complexes **2** and **3** (*vide infra*) are the first 3d transition metal complexes to contain the ligand 2-(acetoxy)phenyl hydroxamic acid (L_1H_2). However, L_1H_2 has been previously used in constructing the heteroleptic ruthenium(III)-hydroxamate complex ([Ru(III)(H_2edta)(L_1H_1)].2H_2O).[10]

The reaction of anhydrous ferric chloride, L_1H_2 and $Bu_4N(OH)$ in acetonitrile produces a red / brown solution from which red X-ray quality crystals of the dinuclear complex [Fe(III)$_2$(L_1H)$_4$$Cl_2$]·2MeCN (**2**) were obtained. Complex **2** crystallises in the triclinic *P*-1 space group (Z = 1). The two Fe(III) centres in **2** are linked by two μ-bridging O_{phen} atoms (O2 and symmetry equivalent (s.e.)) belonging to two singly deprotonated η^1:η^2: μ-bonding L_1H^- ligands (Fe1-O2-Fe1´ = 106.85°). The Fe(III) oxidation state assignments in **2** were confirmed using BVS calculations, bond length and charge balancing considerations (Table S4). The two remaining symmetry related hydroxamate ligands chelate to the metal centres in **2** (O,O´-

bidentate), while terminal Cl^- ligands (Cl1 and s.e.) complete their respective coordination spheres (Fe1-Cl1 = 2.31 Å). Intra-ligand H-bonding interactions are observed within all four L_1H^- ligands, between the hydroxamate N-H groups (H1 and H2) and the juxtaposed methoxide O atoms (O3 and O6) (N1(H1)···O3 = 1.96 Å; N2(H2)···O6 = 2.00 Å) (Fig. 2). Two crystallographically equivalent MeCN solvents of crystallisation lie at the periphery of the structure in **2**, held in position through an intermolecular hydrogen bond between the N donor atom (N3) and a hydroxamate NH group (N2(H2)···N3 = 2.28 Å). This solvent of crystallisation (and s.e.) connects the individual $\{Fe(III)_2\}$ units in **2** through H-bonding with adjacent Cl^- ligands via its $–CH_3$ protons (Cl1···(H18C′)C18′ = 2.82 Å) (Fig. 2-right). These Cl^- ligands also interact with nearby protons belonging to hydroxamate –OMe groups of adjacent $\{Fe(III)_2\}$ complexes (Cl1···(H16B′)C16′ = 2.82 Å).

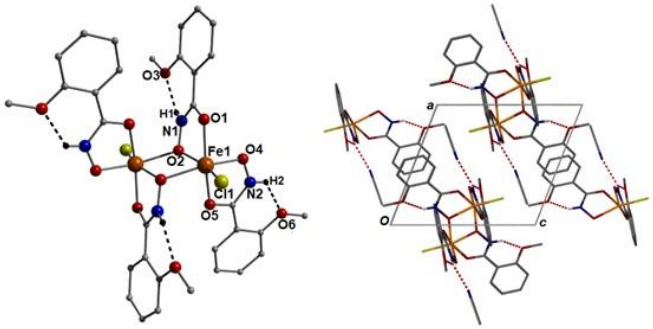

Figure 2 Crystal structure of $[Fe(III)_2(L_1H)_4Cl_2]\cdot 2MeCN$ (**2**) (left) and its corresponding packing arrangement (right) as viewed along the *b* unit cell direction. Dashed lines represent intra-molecular H-bonds (N1(H1)···O3 = 1.96 Å; N2(H2)···O6 = 2.00 Å). Colour code: Orange (Fe), Red (O), Blue (N), grey (C), Light grey (H), Yellow (Cl). The majority of hydrogen atoms have been omitted for clarity.

The methanolic reaction of $Co(II)(NO_3)_2\cdot 6H_2O$, L_1H_2 and $NEt_4(OH)$ gives rise to the crystallisation of the heterovalent heptanuclear complex $[Co(III)Co(II)_6(L_1H)_8(L_1)_2(MeOH)_4(NO_3)_2]NO_3\cdot 3.5H_2O\cdot 14MeOH$ (**3**) (Fig. 3). Complex **3** crystallises in the triclinic *P*-1 space group and possesses a metallic skeleton describing a bicapped trigonal bipyramid. As highlighted in Figure 3c, Co2-Co6 occupy the trigonal bipyramidal core structure, while Co1 and Co7 act as edge caps to the Co2-4 and Co5-6 vertices, respectively. BVS calculations, bond length and charge balancing considerations reveal that Co3 is in the +3 oxidation state, with all other metal centres being divalent (Table S5). The core in **3** is constructed through a combination of eight singly (L_1H^-), and two doubly

(L_1^{2-}) deprotonated 2-(acetoxy)phenyl hydroxamate ligands using the η^1:η^2 μ- (L_1H^-), η^1:η^3 μ_3- (L_1H^-) and η^1:η^3:η^1 μ_4- (L_1^{2-}) bridging modes (Fig. 3). All cobalt centres exhibit distorted octahedral geometries. Terminally bonded methanol ligands complete the coordination spheres at centres Co1, Co4, Co5 and Co7 (Co-O_{MeOH} bond range: 2.06-2.09 Å), while two of the three NO_3^- anions in **3** are bound to the metal ions Co2 and Co6, respectively, at distances of 2.10 Å (Co2-O14) and 2.06 Å (Co6-O25). The eight singly deprotonated L_1H^- ligands remain protonated at their amide N atoms. These protons are involved in intra-ligand interactions through their -OCH_3 groups (*e.g.* N2(H2H)···O13 = 1.96 Å; N8(H8H)···O37 = 1.84 Å and N10(H10H)···O7 = 2.15 Å), as well as with O donor atoms of neighbouring hydroxamate ligands (*e.g.* N2(H2H)···O20 = 2.70 Å; N8(H8H)···O24 = 2.64 Å and N10(H10H)···O36 = 2.43 Å) and NO_3^- counter anions (N1(H1H)···O15 = 2.14 Å). The terminal MeOH ligands in **3** hydrogen bond to nitrate counter anions at distances of (for example): 2.11 Å (O17(H17)···O14) and 2.38 Å (O34(H34)···O25). The individual {Co(III)$Co(II)_6$} units in **3 c**onnect to one another through strongly directional intermolecular H-bonds between terminal MeOH protons (H4H) and O donor atoms (O27) from neighbouring metal bound NO_3^- counter anions (O4(H4H)···O27′ = 1.82 Å). Further connections in the form of C-H···π intermolecular interactions are observed between aromatic hydroxamate protons (*e.g.*. H47) and neighbouring aromatic hydroxamate rings (*e.g.* C47′(H47′)···[C75-C80]$_{centroid}$ = 2.43 Å).

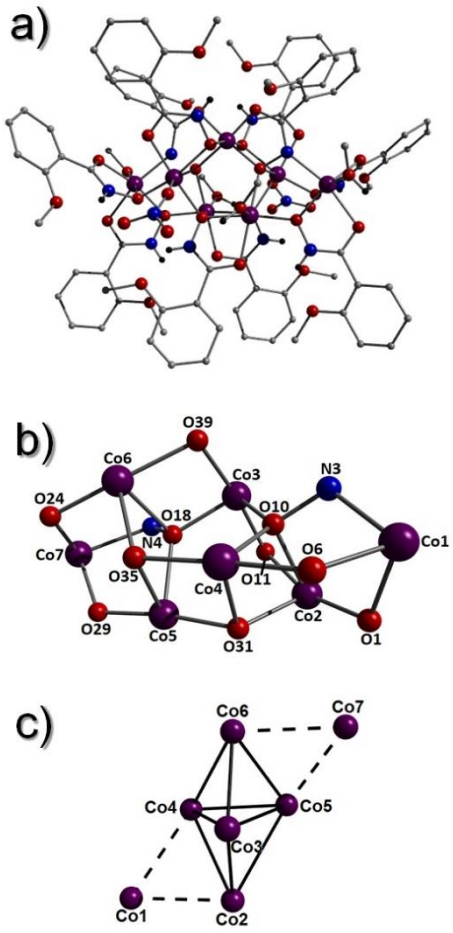

Figure 3 (a) Crystal structure of $[Co(III)Co(II)_6(L_1H)_8(L_1)_2(MeOH)_4(NO_3)_2]NO_3 \cdot 3.5H_2O \cdot 14MeOH$ (**3**). Colour code: Purple (Co), Red (O), Blue (N), Grey (c), Black (H). The unbound nitrate anions and the majority of hydrogen atoms have been omitted for clarity. (b) The inorganic core in **3** including the bridging O / N atoms. (c) The bicapped trigonal bipyramidal topology in **3**. The solid lines highlight the trigonal bipyramidal core (Co2-6) while the two edge capped metal ions (Co1 and Co7) are connected to the core through dashed lines.

The 2D extended network $\{[Cu(II)(L_2H)(H_2O)(NO_3)] \cdot H_2O\}_n$ (**4**) represents the first example of a metal coordination compound built with the L_2H_2 ligand. Crystals of **4** were obtained in the monoclinic $P2_1/c$ space group and its asymmetric unit comprises one Cu(II) centre, one L_2H^- ligand, one NO_3^- anion and a single, terminally bonded water molecule. Each hydroxamate (L_2H^-) ligand chelates to a Cu(II) centre through the hydroxyl and carbonyl atoms O1 and O2, respectively, to give bond lengths of 1.92 Å (Cu1-O1) and 1.94 Å (Cu1-O2). The remaining methoxy oxygen atom (O3) remains unbound and hydrogen bonds with the juxtaposed amide N atom (N1) (N1(H1)···O3 = 2.03 Å). The Cu1 centre in **4** exhibits distorted, Jahn-Teller elongated octahedral geometry, where the basal plane comprises donor atoms from

the chelating hydroxamate ligand, a terminal water ligand (Cu1-O4 = 1.96 Å) and a -NH_2 group from a neighbouring L_3H^- unit (Cu1-N2′ = 2.03 Å). Moreover, the axial positions are occupied by NO_3^- anions (via O5 and O6 respectively) at distances of 2.44 Å (Cu1-O5) and 2.70 Å (Cu1-O6′). The NO_3^- counter anions in **4** connect the Cu(II) ions to form superimposable zig-zag arrays along the *c* direction of the unit cell (Cu1···Cu1′ = 5.70 Å). These 1D rows are connected to one another through the ditopic L_2H^- ligand via their pendant –NH_2 groups (N2-Cu1′ = 2.030 Å) to produce a Cu···Cu1′′ distance of 9.25 Å (Fig.4). The result is the formation of 2D wave-like sheets that propagate along the *ac* plane of the unit cell with an overall [4,4] net topology (Fig. 5a). The individual sheets in **4** pack in a space efficient manner along the *b* direction as highlighted using the colour coded space-fill diagram in Figure 5c. The s.e. waters of crystallisation (O8) lie in the channels forged by the 2D sheets in **4** and are involved in multiple hydrogen bonding interactions with nearby amide (O8···(H1′)N1′ = 2.20 Å) and ligated water protons (O4(H4A)···O8 = 2.01 Å).

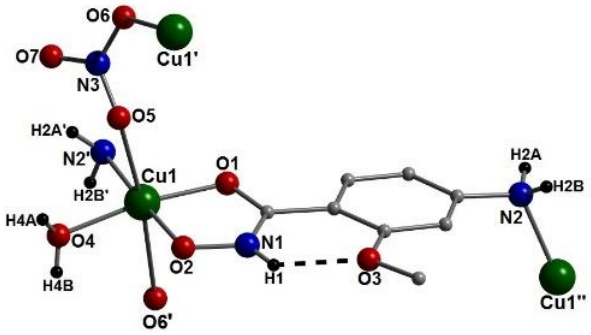

Figure 4 The asymmetric unit in {[Cu(II)(L_2H)(H_2O)(NO_3)]·H_2O}$_n$ (**4**) along with the connector atoms (N2′, O6′, Cu1′ and Cu1′′) that propagate the 2D extended network in **4**. The majority of H atoms and the water of crystallisation have been omitted for clarity. Intramolecular H-bond represented as a dashed line (N1(H1)···O3 = 2.03 Å).

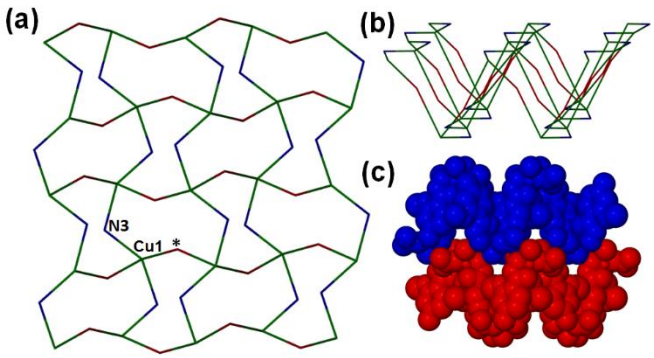

Figure 5 The wave-like [4,4] net topology in 4 as viewed perpendicular (a) and parallel (b) to the plane of the 2D sheets. Note: The green and dark blue nodes represent the Cu(II) centres and the central N atom (N3) of the connector NO_3^- anions, respectively. The red nodes (*) represent the aromatic centroid positions of the ditopic L_2H^- hydraxamate ligands in 4. (c) A space-fill representation of the packing motif between two colour coded wave-like sheets in 4 as viewed along the *c* unit cell direction.

Due to its redundant nature with respect to metal coordination, our next strategy was to replace the -OAc group in L_1H_2 (and L_2H_2) with an methylamino (-NHMe) moiety in the form of the ligand 2-(methylamino)phenyl hydroxamic acid (L_3H_2; Scheme 1). Indeed, this proved successful when the methanolic reaction of Zn(II)$(NO_3)_2\cdot 6H_2O$ and L_3H_2 in the presence of NaOH gave a pale yellow reaction mixture that upon filtration and slow evaporation gave rise to pale yellow crystals of $\{[Zn(II)(L_3H)_2]\cdot 2MeOH\}_n$ (**5**) (Fig. 6). The parallelpiped crystals of **5** were obtained in the orthorhombic *Pcc*2 space group and comprise of Zn(II) ions in distorted octahedral geometry connected into superimposable 1D rows that propagate along the *c* unit cell direction (Fig. 7). The metal centres are linked into the polymeric array via the singly deprotonated $\eta^1{:}\eta^2$ μ-bridging L_3H^- ligands. The hydroxamate ligands in **5** sit alternately above and below the Zn1-O1-Zn1′ plane and form both the equatorial (Zn1-O1 = 2.13 Å and Zn1-O1′ = 2.09 Å) and axial (Zn1-O2 = 2.12 Å) bonds to the metal centres. The crystallographically equivalent methanol solvents of crystallisation lie along the channels formed in between the cubic packed $[Zn(II)(L_3H)_2]_n$ chains and are held in position through H-bonds with nearby hydroxamate O donor atoms (O1 and s.e.) at a distance of 1.94 Å (C9-O3(H3)···O1).

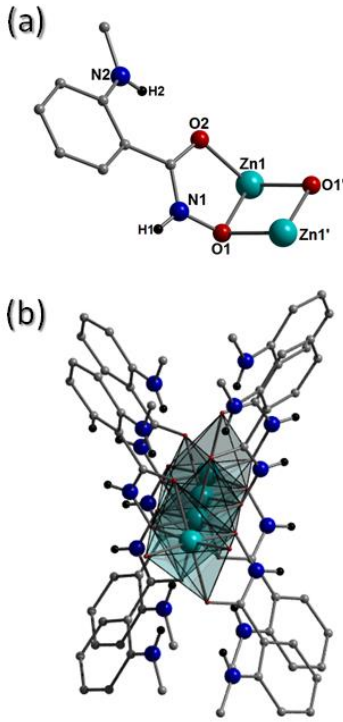

Figure 6 (a) The asymmetric unit in $[Zn(II)(L_3H)_2]_n \cdot 2MeOH$ (**5**) along with the crystallographically related Zn1´ and O1´ atoms. Colour code: Light blue (Zn), Red (O), Dark blue (N), Grey (C), Black (H). (b) A 1D row in **5** as viewed off-set along the *c* unit cell direction.

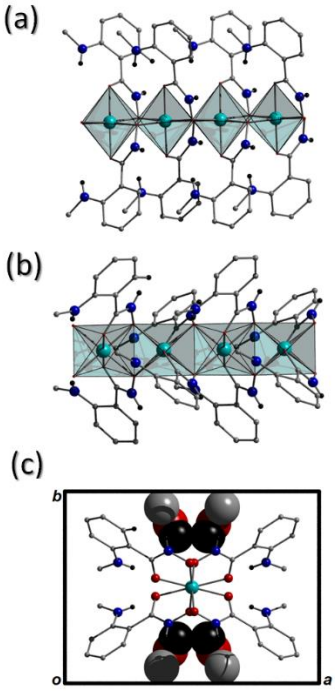

Figure 7 A polyhedral representations of the 1D-chains as viewed along the equatorial (a) and axial (b) planes of the distorted octahedral Zn(II) centres in **5**. (c) The unit cell in **5** as viewed along the *c* direction. The methanol solvents of crystallisation are shown in space-fill mode.

The methanolic reaction of $Cu(NO_3)_2 \cdot 3H_2O$, ligand L_3H_2 and NaOH gave rise to a green solution which after filtration and slow evaporation produced dark green block-like crystals of $[Cu(II)_5(L_3)_4(NO_3)_2]\cdot 3H_2O$ (**6**). The asymmetric unit in **6** comprises two half $\{Cu_5\}$ units (labelled Cu1-Cu3 and Cu4-Cu6, respectively) and are separated by 2.95 Å (Cu4···N4') at the shortest distance. The inorganic cores in **6** comprises a body centred square array of Cu(II) ions joined together through four $\eta^1{:}\eta^2{:}\eta^1{:}\eta^1$ μ_3- bridging L_3^{2-} ligands to forge a 12-MC-4 metallacrown topology (Fig. 8).[7b] The central Cu(II) ions exhibit distorted octahedral (Cu1) and distorted square planar (Cu6) geometries, respectively. The axial contacts at Cu1 are made by two symmetry equivalent μ-bridging NO_3^- anions (Cu1-O5 = 2.43 Å), that also provide the axial contacts at the two symmetry equivalent Cu3 centres (Cu3-O7 = 2.64 Å). The two NO_3^- anions belonging to the second crystallographically unique $\{Cu(II)_5\}$ moiety are located at the axial positions of the outer (distorted square based pyramidal) Cu(II) ions (Cu5 and s.e.) at a distance of 2.42 Å (Cu5-O12). The remaining metal centres (Cu2, Cu4) in both pentametallic units exhibit distorted square planar geometries, although the Cu2 centres are provided with long contact at the axial positions with O_{phen} atoms (O10 and s.e.) of the nearby second $\{Cu(II)_5\}$ unit (Cu2···O10' = 2.91 Å). The waters of crystallisation in **6** (O17-O19) are held in position through numerous H-bonding interaction with O donor atoms and secondary amine and aromatic protons belonging to L_3^{2-} units (*e.g.* O3···O17 = 2.74 Å; N2(H2)···O17 = 1.99 Å; C3(H3)···O18 = 3.14 Å and C13(H13)···O19 = 2.76 Å). The individual pentametallic units in **6** pack in a brickwork manner along the *ab* plane of the unit cell and the resultant 2D sheets stack in parallel and superimposable rows along the *c* axis of the unit cell (Fig. S3).

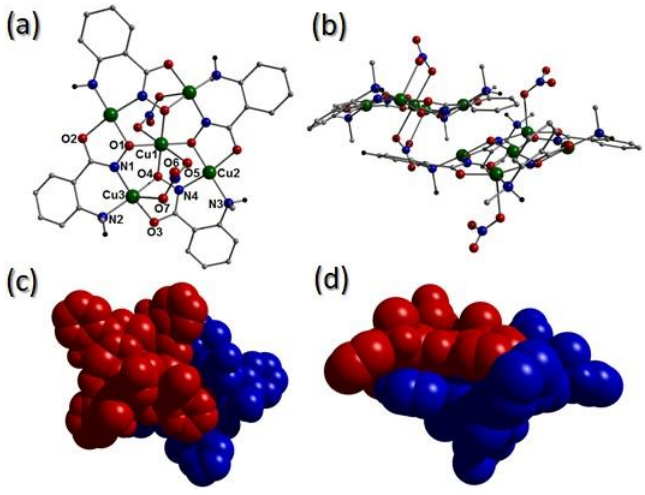

Figure 8 (a) The crystal structure in $[Cu(II)_5(L_3)_4(NO_3)_2]\cdot 3H_2O$ (**6**) as viewed perpendicular to the pentametallic core. (b) The two $[Cu_5]$ units grown from the ASU in **6** represented in traditional (b) and

colour coded space-fill modes as viewed perpendicular (c) and parallel (d) to their pentametallic inorganic cores. The majority of hydrogen atoms and all waters of crystallisation have been removed for clarity.

The Zn(II) coordination polymer in **5** along with the 12-MC-4 metallacrown in **6** represent the first 3d transition metal complexes to be constructed using L_3H_2. Lipczynska-Kochany and co-workers have previously synthesised L_3H_2 to examine the Lossen rearrangement of hydroxamic acids and more broadly, on the biological activities of hydroxamic acids.[11] Iwamura and co-workers have probed the fluorescence properties of 2-(methylamino)phenyl hydroxamic acid (L_3H_2).[12] Furthermore, Sianesi and Bonola used L_3H_2 as part of their research into using a series of 3-hydroxy-2,3-dihydro-4(1H)-quinazoline derivatives (produced via the ring closure of certain hydroxamic acids), for potential use as antibacterial and antifungal agents.[13]

Some of our previous work has entailed the in-situ formation (and Cu(II) ligation) of a series of ligands constructed from the Schiff base coupling of 2-amino-phenylhydroxamic acid and o-vanillin (and its analogues). The planarity of the resulting ligands (such as o-[(E)-(2-hydroxy-3-methoxyphenyl)methylideneamino]benzohydroxamic acid in Scheme 2), gave rise to a family of layered planar cages ranging in nuclearity from $[Cu_{10}]$ to $[Cu_{30}]$.[14] Selectively reducing the imine group of the o-[(E)-(2-hydroxy-3-methoxyphenyl)methylideneamino]benzohydroxamic acid ligand affords (*N*-hydroxy-2-((2-hydroxy-3-methoxybenzyl)amino)benzamide (L_4H_3; Scheme 2). The introduction of a secondary amine group should render the resultant ligand non-planar and the effect of this structural change would be observable upon subsequent metal complex formation. The target ligand (*N*-hydroxy-2-((2-hydroxy-3-methoxybenzyl)amino)benzamide (L_4H_3) was successfully synthesised by the one-pot Schiff base coupling and selective imine reduction of 2-amino-phenylhydroxamic acid and ortho-vanillin using the reducing agent sodium triacetoxyborohydride.[15]

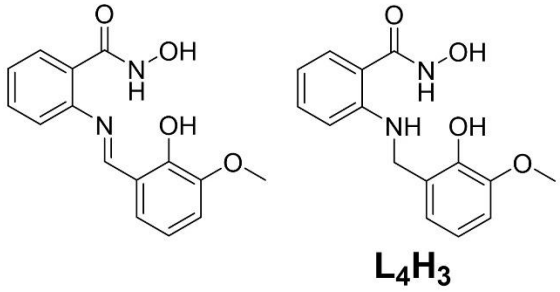

L_4H_3

Scheme 2: (Left) The ligand o-[(E)-(2-hydroxy-3-methoxyphenyl)methylideneamino]benzohydroxamic acid previously used in the production of a series of polynuclear Cu(II) complexes ([$Cu(II)_{10}$], [$Cu(II)_{14}$] and [$Cu(II)_{30}$]).[14] (Right): The novel ligand (*N*-hydroxy-2-((2-hydroxy-3-methoxybenzyl)amino)benzamide (L_4H_3) used in this work.

The methanolic reaction of L_4H_3 with $Cu(NO_3)_2 \cdot 3H_2O$ and NaOH gives rise to the pentametallic complex $[Cu(II)_5(L_4H)_4(MeOH)_2(NO_3)_2] \cdot 3H_2O \cdot 4MeOH$ (**7**), that crystallises in the triclinic *P*-1 space group. Akin to **6**, the pentametallic core in **7** comprises a planar 12-MC-4 metallacrown topology, where the central, distorted square planar Cu centre (Cu1) is surrounded by a square of four other copper ions (Cu2-3 and s.e.) (Fig. 9a). The five metal centres in **7** are bonded by four doubly deprotonated L_4H^{2-} ligands, each exhibiting an $\eta^1:\eta^2:\eta^1:\eta^1:\eta^1$ μ_3-bridging mode (Fig. 9d). More specifically, the planar $\{Cu(II)_5\}$ core in **7** is formed due to metal ligation to the near planar hydroxamate groups of each L_4H^{2-} ligand, as observed in previous 12-MC-4Cu(II) metallacrowns.[9] However, unlike in other analogues, the deliberate introduction of the secondary amine groups provides each ligand with a natural kink, which results in each the four independent ligand phenolic groups to significantly deviate from the $\{Cu(II)_5\}$ plane (Fig. 9c).

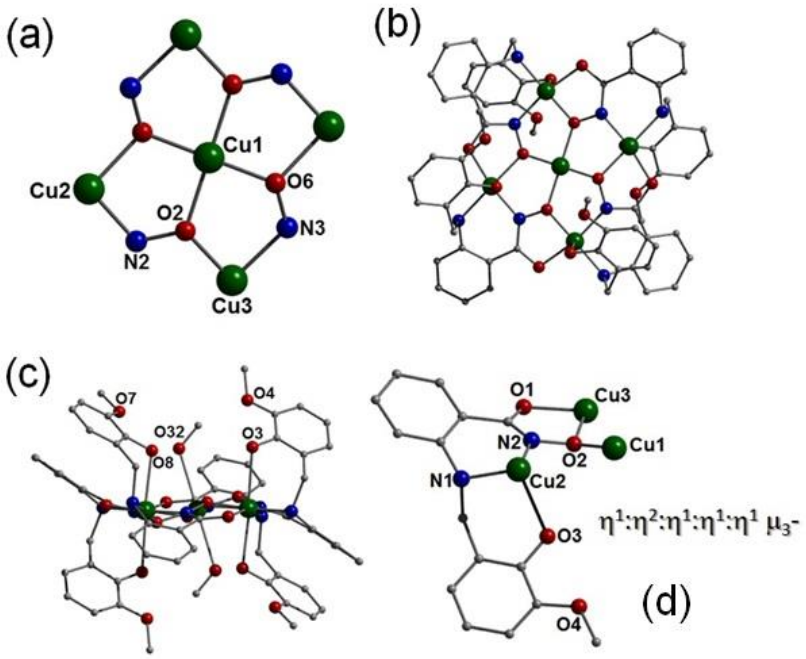

Figure 9 (a) The inorganic core in $[Cu(II)_5(L_4H)_4(MeOH)_2](NO_3)_2 \cdot 3H_2O \cdot 4MeOH$ (**7**) along with the crystal structure of **7** as viewed perpendicular (a) and parallel (b) to the $\{Cu(II)_5\}$ plane. The terminal MeOH ligand at Cu1 has been omitted for clarity. All hydrogen atoms have been omitted for clarity. (d) The bonding mode exhibited by the L_4H^{2-} ligands in **7**. The bold line represents an elongated axial Cu-O interaction (Cu2-O3 = 2.502 Å).

As a result, these phenolic units sit in an up-up-down-down arrangement with respect to the planar core in **7** and are therefore able to forge long axial contacts with the four outer Cu centres (Cu2-O3 = 2.50 Å and Cu3-O8B = 2.50 Å; Fig. 9c). This gives rise to a distorted square based pyramidal geometry at Cu2 (τ_{Cu2} = 0.10) and a distorted octahedral geometry at Cu3 (due to a long sixth contact with a nearby NO_3^- counter anion; Cu3-O10 = 2.72 Å). It should be noted that the aromatic hydroxamate rings also deviate away from the $\{Cu(II)_5\}$ plane but to a lesser extent. Two terminal ligated MeOH ligands occupy the axial positions at the central distorted octahedral Cu1 site (Cu1-O32 = 2.65 Å) and effectively sit in a pocket forged by the aforementioned phenolic groups of the L_4H^{2-} ligands in **7**. Numerous parallel-displaced π-π stacking interactions between the hydroxamate aromatic rings of each L_4H^{2-} moiety aid the space efficient packing observed in the unit cell of **7** (e.g. $[C2\text{-}C7]_{centroid}\cdots[C2'\text{-}C7']_{centroid}$ = 3.78 Å) (Fig. S4).

Magnetic studies

The dc (direct current) molar magnetic susceptibility, χ_M, of polycrystalline samples of $[Fe(III)_2(L_1H)_4Cl_2]\cdot 2MeCN$ (**2**),

$[Co(III)Co(II)_6(L_1H)_8(L_1)_2(MeOH)_4(NO_3)_2]NO_3 \cdot 3.5H_2O \cdot 14MeOH$ (**3**), and $[Cu(II)_5(L_4H)_4(MeOH)_2](NO_3)_2 \cdot 3H_2O \cdot 4MeOH$ (**7**) were measured in an applied magnetic field, *B*, of 0.1 T for **2** and **3**, and 0.5 T for **7**, in the *T* = 300-2 K temperature range. The experimental results are shown in Figure 10 in the form of the $\chi_M T$ products, where $\chi = M/B$, and *M* is the magnetisation of the sample.

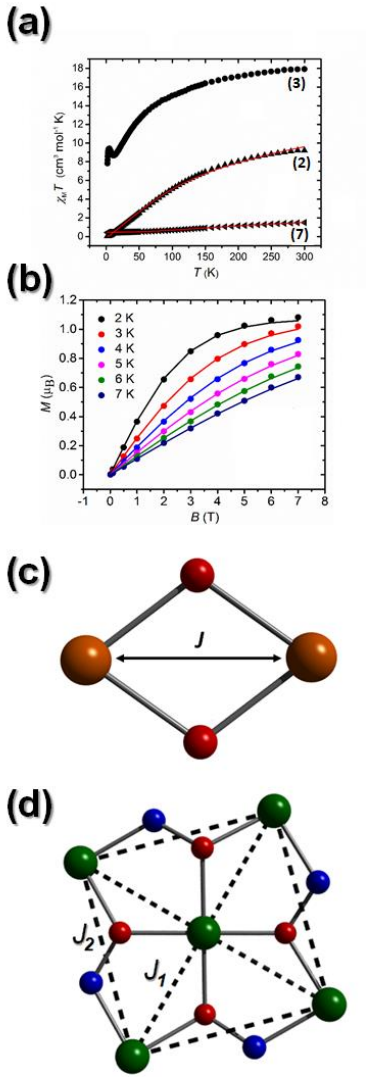

Figure 10 (a) Overlay $\chi_M T$ versus *T* plots for polycrystalline sample of **2**, **3**, and **7** taken in the *T* = 300-2 K temperature range in an applied field, *B*, of 0.1 T for **2** and **3**, and 0.5 T for **7**. (b) Magnetisation (M/μ_B) vs. *B* (T) data obtained from a polycrystalline sample of **7** measured in the 2-7 K temperature range and 0-7 T magnetic field range. (c and d) The exchange coupling schemes used to fit the data in **2** (c) and **7** (d). For **2**; $\hat{H} = -2J(\hat{S}_1 \cdot \hat{S}_2)$ and for **7**; $\hat{H} = -2J_1(\hat{S}_1 \cdot \hat{S}_5 + \hat{S}_2 \cdot \hat{S}_5 + \hat{S}_3 \cdot \hat{S}_5 + \hat{S}_4 \cdot \hat{S}_5) -2J_2(\hat{S}_1 \cdot \hat{S}_2 + \hat{S}_2 \cdot \hat{S}_3 + \hat{S}_3 \cdot \hat{S}_4 + \hat{S}_4 \cdot \hat{S}_1)$. The solid lines represent a simultaneous best-fit of the experimental susceptibility and magnetisation data as described in the main text. Colour code as described earlier in the text.

For **2**, the $\chi_M T$ product of 9.21 cm^3 mol^{-1} K at 300 K is close to that expected for two non-interacting Fe(III) ions (8.75 cm^3 mol^{-1} K), assuming g_{Fe} = 2.0, where g_{Fe} is the *g*-factor of Fe(III). The corresponding $\chi_M T$ product of 1.49 cm^3 mol^{-1} K for **7** is significantly lower than the expected value for five Cu(II) ions (2.17 cm^3 mol^{-1} K, when g_{Cu} = 2.14) As shown in Figure 10, the $\chi_M T$ vs. *T* plots in both cases show a decrease in the value of $\chi_M T$ upon cooling and are indicative of significant intramolecular antiferromagnetic exchange interactions between the Fe(III) and Cu(II) ions in **2** and **7**, respectively. The magnetic data for both **2** and **7** were fit using the program PHI and an isotropic spin-Hamiltonian of the form: [16]

$$\hat{H} = -2\sum_{i,j>i}^{n} \hat{S}_i J_{ij} \hat{S}_j + \mu_B \sum_{i=1}^{n} \vec{B}\, g_i \hat{S}_i$$

where $\hat{S}$ is a spin operator, *J* is the pairwise isotropic magnetic exchange interaction between constitutive metal centres, μ_B is the Bohr magneton, $\vec{B}$ the external static magnetic field, *g* the isotropic *g*-factor of the metal ions, the indices *i* and *j* refer to the constituent metal ions (n = 2 for **2**, and n = 5 for **7**).

The best fit parameters for **2** are *J* = -7.34 cm^{-1} and g_{Fe} = 2.00, consistent with previously reported analogues.[17] There are two separate magnetic exchange interactions between the Cu(II) centres in **7** (Fig. 10), $Cu(II)_{outer}$-$Cu(II)_{inner}$ (comprising 1 x Cu-O_{oxime}-Cu bridge; J_1) and $Cu(II)_{outer}$-$Cu(II)_{outer}$ (comprising 1 x Cu-N-O-Cu bridge; J_2). A simultaneous fit of the susceptibility and magnetisation data affords best-fit parameters g_{Cu} = 2.14, J_1 = -115.33 cm^{-1} and J_2 = -83.03 cm^{-1}. The *J*-values obtained are in line with those observed in other similarly bridged Cu(II) complexes[9,18] and give rise to an isolated *S* = 1/2 ground spin state.

The $\chi_M T$ value for **3** at 300 K is 17.93 cm^3 mol^{-1} K, higher than that expected for six non-interacting Co(II) ions (*S* = 3/2, g_{Co} = 2.3, $\chi_M T$ = 14.88 cm^3 mol^{-1} K).[19] On cooling, the value of $\chi_M T$ decreases to approximately 8.68 cm^3 mol^{-1} K at 12 K before increasing to 9.41 cm^3 mol^{-1} K at 5 K, and decreasing to a value of 7.84 cm^3 mol^{-1} K at 2 K. The initial decrease in the value of $\chi_M T$ can be attributed to the large orbital contribution of the high spin octahedral Co(II) ions and/or antiferromagnetic exchange interactions. The increase between 12-5 K indicates the presence of some ferromagnetic exchange interactions, and the low *T* decrease due to zero-field splitting effects and/or antiferromagnetic intermolecular interactions. Quantitative analysis of the data is precluded by the large first order spin orbit coupling contribution associated with the octahedral Co(II) ions. No out-of-phase alternating current (ac) signals were observed for **3**, even in the presence of an applied magnetic field.

UV-Vis absorption and photoluminescence spectra of complex 5

Complex $\{[Zn(II)(L_3H)_2]\cdot 2MeOH\}_n$ (**5**) showed blue fluorescence upon UV irradiation, which prompted a more detailed UV-Vis absorption and fluorescence study as described below. Absorption spectra demonstrated two distinct maxima at ca. 255 – 258 nm and 341 – 351 nm (Fig. 11a and Table 1). The longest wavelength absorption maxima are only slightly shifted upon solvent variation, while no correlation with respect to solvent polarity is observed. A Drop-casted film of **5** shows an absorption in the same region (346 nm), thus there is no solid-state effect on the electronic ground state of the complex.

Photoluminescence (PL) spectra show that in all solvents, complex **5** emits in the blue region with PL maxima of λ_{PL} = 421 – 433 nm (Figures 11b and S6) (Table 1). Thus, the solvent effect on the excited state is comparable to that of the ground state. Again, while there are obvious changes (but not large) in PL maxima with solvent change, they do not correlate with the polarity of the solvent, reflecting that while solvation is an important factor, it cannot be assigned just to changes in the intra-chain charge transfer in **5**. We should also mention that for all solvents, the emission of the complex is bathochromically shifted compared to that of the free ligand L_3H_2 (Table 1).

In contrast to the absorption spectra PL spectra for both thin films and powder demonstrate bathochromic shifts (by ca. 15 – 30 nm, as estimated at their half maxima) with an appearance of two distinct emission bands. This indicates a stabilisation of the excited state of the complex due to intermolecular interactions. However, no broadening of the PL spectra is observed and the emission bands show only small changes in their fwhm (full width at half maximum) in the range of 0.432 – 0.478 eV (Table 1).

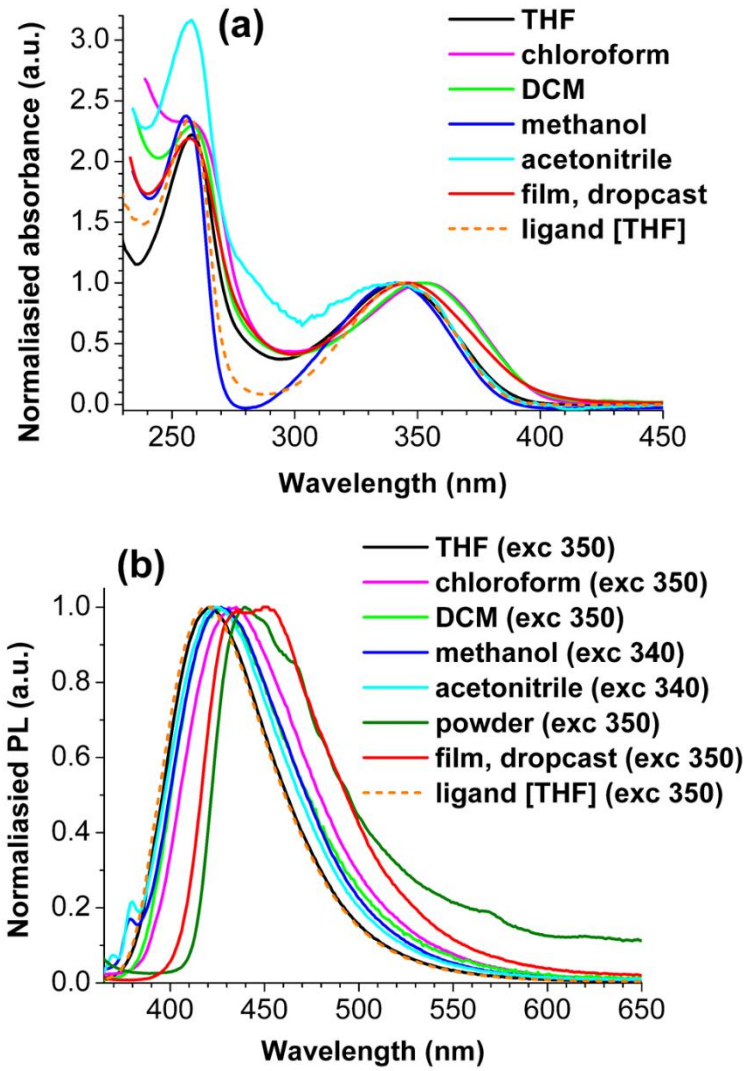

Figure 11 UV-Vis absorption (a) and photoluminescence (b) spectra of complex **5** and ligand L_3H_2 in different solvents and in the solid state. Excitation wavelengths for PL spectra are given in brackets. UV-Vis absorption spectra are normalised to the longest wavelengths maxima.

Table 1 Absorption and emission maxima of complex **5** in different solvents and in the solid state, together with data for ligand L_3H_2.

Solvent (or solid state)	**ε[a]**	**λ_{abs} (nm)**	**λ_{PL} (nm)[b]**	**fwhm (eV)[c]**
Ligand L_3H_2 (in THF)	37.5	257, 344	419	0.448
Chloroform	4.81	256sh, 353	433	0.473
Tetrahydrofuran	7.58	258, 342	421	0.446
Dichloromethane	8.93	258.5, 351	426	0.474
Methanol	32.7	255.5, 341	427	0.478
Acetonitrile	37.5	258, 342	425	0.475
Film (drop-casted)	–	257, 346	436, 450	0.465
Powder	–	–	440, 460sh	0.432

[a] Dielectric permittivity of the solvent. [b] Excitation maxima are shown on Fig. 11b. [c] Full width at half maximum of the emission spectra.

Conclusions

We have presented a number of novel mono- and polymetallic complexes constructed using a family of related mono- and ditopic hydroxamic acid ligands. For instance, the ligands 4-amino-2-(acetoxy)phenyl hydroxamic acid (L_2H_2) and *N*-hydroxy-2-[(2-hydroxy-3-methoxybenzyl)amino]benzamide (L_4H_3) were employed in the construction of the 2-D extended network $\{[Cu(II)(L_2H)(H_2O)(NO_3)].H_2O\}_n$ (**4**; L_2H_2 = 4-amino-2-(acetoxy)phenyl hydroxamic acid) and the discrete 12-MC-$4_{Cu(II)}$ metallacrown $[Cu(II)_5(L_4H)_4(MeOH)_2(NO_3)_2]\cdot 3H_2O\cdot 4MeOH$ (**7**), respectively. Complex **7** represents the first complex to be constructed with the L_4H_3 ligand. Moreover, the ferric dimer $[Fe(III)_2(L_1H)_4Cl_2]\cdot 2MeCN$ (**2**) and the H-bonded 1-D coordination polymer $\{[Zn(II)(L_3H)_2]\cdot 2MeOH\}_n$ (**5**) represent extremely rare examples of metal coordination of the ligands 2-(acetoxy)phenyl hydroxamic acid (L_1H_2) and 2-(methylamino)phenyl hydroxamic acid (L_3H_2). Variable temperature magnetic susceptibility measurements on **2** and **7** indicate dominant antiferromagnetic exchange in both cases, with best-fit-data for **2** and **7** J = -7.34 cm^{-1}, and J_1 = -115.33 cm^{-1}, J_2 = -83.03 cm^{-1}, respectively. In solution, coordination polymer complex **5** exhibits an emission in the blue region with $\lambda_{PL} \approx 421 – 433$ nm depending on the solvent. While very small effects are observed upon absorption and PL spectra of **5** in solution, a bathochromic shift of ≈ 15 – 30 nm is observed for its photoluminescence in the solid state, underlying the importance of inter-chain interactions on the excited state of the complex.

Conflicts of interest

There are no conflicts to declare.

Acknowledgements

We would like to thank the School of Natural Sciences at Bangor University for their support (LFJ, RE and BFM). BFM would also like to thank the University of Maiduguri and the Petroleum Technology Development Fund (PTDF) for their award of an overseas fellowship. We would like to thank the EPSRC National Crystallographic Service and EPSRC UK National Mass Spectrometry Facility at Swansea University for their support. EKB thanks the EPSRC (EP/N01331X/1, EP/P025986/1) for support.

Experimental information

Infra-red spectra were recorded on a Perkin Elmer FT-IR *Spectrum 100* spectrometer. ^{1}H and ^{13}C NMR spectra were obtained at room temperature (298 K) on a Bruker Avance 400 Plus spectrometer with Sample Xpress, operating at 400 MHz (for ^{1}H) or 100 MHz (for ^{13}C). Chemical shifts are reported in ppm and referenced to DMSO-d_6 (δ_H: 2.50 ppm, δ_C : 39.52 ppm). Elemental analysis was carried out at OEA Laboratories (Kelly Bray, Cornwall). Room temperature magnetic moment measurements were taken on a Johnson Matthey balance (reference material: $HgCo(NCS)_4$). Variable-temperature, solid-state direct current (*dc*) and alternating current (ac) magnetic susceptibility data down to 2 K were collected on a Quantum Design MPMS-XL SQUID magnetometer and a Quantum Design PPMS magnetometer fitted with an ac measurement system, respectively. Diamagnetic corrections were applied to the observed paramagnetic susceptibilities using Pascal's constants. All measured complexes were set in eicosane to avoid torqueing of the crystallites. All magnetic samples are collected as single-crystalline products and analysed using microanalysis and IR measurements prior to their magnetic assessment. If necessary, phase purity between cross-batches was validated using unit cell checks and IR measurements. Yields calculated upon collection of single-crystalline products in order to ensure high quality magnetic data. UV-Vis spectra on $\{[Zn(II)(L_3H)_2].2MeOH\}_n$ (**5**) were recorded on a Shimadzu (UV-3600) UV-Vis-NIR spectrophotometer at room temperature. Solution measurements in solvents of different polarities (hexane, chloroform, dichloromethane, tetrahydrofyran, acetonitrile, methanol) were carried out in 10 mm path length square quartz cells. For solid state measurements, the solutions

in chloroform were drop-casted onto a quartz circular window, allowed to evaporate slowly and dried *in vacuo*. Photoluminescence spectra (PL) were recorded on a HORIBA Jobin-Yvon Fluoromax-4 spectrofluorometer at room temperature. The solution spectra were measured in 10 mm path length quartz cells for diluted solutions (with absorption at longest wavelength of < 0.1 a.u.). Solid-state PL measurements were performed either for drop-casted film on a quartz substrate or for powder (in a d = 3 mm cylindrical quartz cell, using an integrating sphere Horiba F-3018 on the spectrofluorometer). The samples were excited at λ_{exc} = 340 – 350 nm, close or equal to the maxima of their longest wavelength absorption.

Single-crystal X-ray crystallography

Complexes **1-7** were collected on an Rigaku AFC12 goniometer equipped with an enhanced sensitivity (HG) Saturn724+ detector mounted at the window of an FR-E+ Super Bright molybdenum rotating anode generator with HF Varimax optics (100m focus). (CCDC numbers: 1907525-1907531). The cell determination and data collection of each complex was carried out using the CrystalClear-SM Expert package (Rigaku, 2012). Each data reduction, cell refinement and absorption correction were carried out using CrysAlisPro software (Rigaku OD, 2015),[20] while all structures were solved and refined using SHELXT and SHELXL-2018.[21]

In complexes $[Cu(II)(L_1H)_2]$ (**1**), $[Fe(III)_2(L_1H)_4Cl_2].2MeCN$ (**2**) and $\{[Zn(II)(L_3H)_2].2MeOH\}_n$ (**5**) all hydrogens were assigned to calculated positions while all non-hydrogen atoms were refined anisotropically. Despite numerous attempts, each single crystal data set obtained from $[Co(III)Co(II)_6(L_1H)_8(L_1)_2(MeOH)_4(NO_3)_2]NO_3{\cdot}3.5H_2O{\cdot}14MeOH$ (**3**) were found to consistently diffract poorly at higher angles. The best data set has been supplied in this work. Residual electron densities in solvent accessible voids and channels were observed in **3** (void volume ~ 2105 $Å^3$) and so were modelled using the SQUEEZE program (electron count = 639) to give the final formula.[22] Despite every effort, attempts at modelling the unbound nitrate anion proved futile and so its associated electron density was incorporated into the SQUEEZE calculation. All non hydrogen atoms were refined anisotropically, while all hydrogen atoms were assigned to calculated positions.

All non-hydrogen atoms in $\{[Cu(II)(L_2H)(H_2O)(NO_3)].H_2O\}_n$ (**4**) and $[Cu(II)_5(L_3)_4(NO_3)_2]{\cdot}3H_2O$ (**6**) were refined as anisotropic. The waters of crystallisation in both

complexes were refined isotropically. All hydrogen atoms in **4** and **6** were assigned to calculated positions.

Disorder was observed when refining the crystal structure in $[Cu(II)_5(L_4H)_4(MeOH)_2(NO_3)_2]\cdot 3H_2O\cdot 4MeOH$ (**7**). More specifically, one of the phenolic units belonging to one of the crystallographically unique L_4H^- ligands in **7** required modelling over two sites (50:50 occupancy using the PART function). These disordered atoms required isotropic refinement and DFIX and FLAT restraints, while all other non-hydrogen atoms belonging to the $[Cu_5]$ unit were refined anisotropically. Moreover, the bound MeOH ligand (C46-O32) in **7** was restrained using the DFIX function. The SQUEEZE program was employed to account for the residual electron densities in the solvent accessible voids in **7**. A total void volume of 299 $Å^3$ and an electron count of 102 is commensurate with the final formula: $\mathbf{7}\cdot 3H_2O\cdot 4MeOH$.

Preparation of Complexes 1-7

All reactions were performed under aerobic conditions and all reagents and solvents were used as purchased. ***Caution:*** Although no problems were encountered in this work, care should be taken when manipulating the potentially explosive nitrate salts. For ligand synthesis details see ESI.

*$[Cu(II)(L_1H)_2]$ (**1**)*

$Cu(NO_3)_2.3H_2O$ (0.25 g, 1.034 mmol), 2-(acetoxy)phenyl hydroxamic acid (L_1H_2) (0.17 g, 1.04 mmol) and NaOH (0.04 g, 1.04 mmol) were dissolved in methanol (25 cm^3) and stirred at room temperature for 4 h. The resultant green solution was subsequently filtered and X-ray quality crystals of **1** were obtained upon slow evaporation after one week in 49% yield. Elemental analysis (%) calculated as **1** ($C_{16}H_{16}N_2O_6Cu_1$): C 48.55, H 4.07, N 7.07. Found: C 48.93, H 4.16, N 7.08. FT-IR (cm^{-1}): 3463 (b), 3258 (m), 2979 (w), 3945 (w), 2843 (m), 2494 (w), 2045 (w), 1965 (w), 1802 (w), 1749 (w), 1606 (s), 1562 (m), 1511 (s), 1467 (s), 1425 (m), 1384 (m), 1314 (m), 1294 (w), 1248 (s), 1186 (m), 1166 (m), 1147 (s), 1108 (s), 1019 (s), 985 (m), 929 (s), 858 (w), 824 (w), 809 (w), 770 (s), 750 (s), 709 (m), 677 (s), 633 (s), 532 (m), 485 (m), 421 (m).

*$[Fe(III)_2(L_1H)_4Cl_2]\cdot 2MeCN$ (**2**)*

Anhydrous $FeCl_3$ (0.25 g 1.54 mmol), 2-(acetoxy)phenyl hydroxamic acid (L_1H_2) (0.25 g, 1.54 mmol) and $Bu_4N(OH)$ (0.40 g, 1.54 mmol) were dissolved in MeCN (40 cm^3) and the solution stirred for 4 hours. The resultant red / brown solution was filtered and red X-ray quality of **2**

were obtained in 14% yield after 2 weeks. Elemental analysis (%) calculated as **2** ($C_{32}H_{32}N_6O_{12}Cl_2Fe_2$): C 45.37, H 3.81, N 6.61. Found: C 45.38, H 3.86, N 6.49. FT-IR (cm^{-1}): 3436 (br), 3075 (w), 3002 (m), 2941 (m), 2838 (m), 1606 (s sh), 1590 (m), 1561 (s, sh), 1514 (w), 1488 (s), 1464 (w), 1450 (s), 1435 (s), 1396 (s, sh), 1301 (s), 1275 (s), 1250 (s), 1179 (s), 1051 (w), 1042 (s), 1022 (s), 949 (w), 851 (s), 806 (m), 783 (w), 758 (s, sh), 697 (s), 658 (s,),629 (s) 572 (m), 530 (m), 473 (s), 429 (m).

*$[Co(III)Co(II)_6(L_1H)_8(L_1)_2(MeOH)_4(NO_3)_2]NO_3{\cdot}3.5H_2O{\cdot}14MeOH$ (**3**)*

$Co(NO_3)_2.6H_2O$ (0.25 g, 0.86 mmol), *N*-hydroxy-2-methoxybenzamide (L_1H_2) (0.25 g, 1.54 mmol) and tetraethylammoniumhydroxide (NEt_4OH) (0.08 g, 1.54 mmol) were dissolved in MeOH (30 cm^3) and stirred for 4 hrs at room temperature. The resultant dark purple solution was subsequently filtered and X-ray quality crystals of **3** were obtained upon Et_2O diffusion in 20% yield. Elemental analysis (%) calculated as **3**.2.5H_2O ($C_{96}H_{150}N_{13}O_{59}Co_7$): C 40.56, H 5.32, 6.41. Found: C 40.33, H 5.38, N 7.33. FT-IR (cm^{-1}): 3327 (br), 2942 (w), 2839 (w), 1597 (s), 1560 (s), 1509 (s), 1477 (s), 1461 (w), 1434 (s), 1373 (s), 1294 (s), 1240 (s), 1180 (s), 1162 (s,), 1149 (s), 1105 (s), 1056 (s), 1013 (m), 957 (s), 911 (w), 865 (s), 774 (s), 751 (s), 725 (s), 689 (w), 667 (w), 622 (s), 603 (s), 562 (s), 522 (s), 500 (s),433 (s).

*$\{[Cu(II)(L_2H)(H_2O)(NO_3)].H_2O\}_n$ (**4**)*

$Cu(NO_3)_2.3H_2O$ (0.25 g, 1.034 mmol), 4-amino-N-hydroxy-2-methoxybenzamide (L_2H_2) (0.18 g, 1.035 mmol) and tetrabutylammonium hydroxide (0.268 g, 1.025 mmol) were dissolved in methanol (20 cm^3) and stirred at room temperature for 4 h. The resultant green solution was subsequently filtered and X-ray quality crystals of **4** were obtained upon slow evaporation of the mother liquor (25% yield). Elemental analysis (%) calculated as $[Cu(II)(L_2H)(H_2O)(NO_3)]_n$ ($C_8H_{11}N_3O_7Cu_1$): C 29.59, H 3.41, N 12.94. Found: C 29.07, H 3.83, N 12.98. FT-IR (cm^{-1}): 3377 (s), 3305 (br), 3219 (s), 3124 (w), 2977 (w), 2838 (w), 22361 (w), 2241 (w), 2201 (w), 2188 (w), 2147 (w), 2100 (w), 2062 (w), 2019 (w), 2008 (w), 1940 (w), 1886 (w), 1601 (s, sh), 1573 (s), 1519 (s), 1472 (s), 1429 (w), 1386 (s), 1330 (w), 1307 (m), 1281 (w), 1260 (s), 1200 (s), 1179 (s), 1151 (s), 1112 (s), 1065 (s), 1025 (s, sh), 951 (s), 904 (s), 851 (s), 838 (m) 821 (m), 753 (w), 734 (s), 704 (m), 654 (s), 583 (s), 553 (s), 535 (w), 461 (s), 431 (s).

*$\{[Zn(II)(L_3H)_2].2MeOH\}_n$ (**5**)*

$Zn(NO_3)_2.6H_2O$ (0.25 g, 0.85 mmol), *N*-hydroxy-2-(methylamino)benzamide (L_3H_2) (0.14 g, 0.85 mmol and NaOH (0.033 g, 0.85mmol) were stirred in methanol (30 cm^3) for 4 hrs. The resultant pale yellow solution was then filtered and X-ray quality crystals of **5** were obtained

upon slow evaporation of the mother liquor in 18% yield. Elemental analysis (%) calculated as **5** ($C_{18}H_{26}N_4O_6Zn_1$): C 47.02, H 5.70, N 12.18. Found: C 47.08, H 4.78, N 12.71. FT-IR (cm^{-1}): 3378 (s), 3270 (br), 3073 (w), 2936 (w), 2814 (m), 2166 (w), 2123 (w), 2010 (w), 1942 (w), 1612 (s, sh), 1572 (s, sh), 1505 (s, sh), 1475 (m), 1452 (m), 1420 (s), 1354 (m), 1324 (s), 1283 (s), 1221 (s), 1173 (s), 1146 (s), 1101 (s), 1066 (s, sh), 1024 (w), 940 (s), 902 (s), 842 (s), 803 (s), 776 (m), 748 (s, sh), 697 (s), 666 (s), 627 (m), 604 (m) 556 (m), 528 (m), 501 (m), 460 (s) 432 (m), 410 (m).

$[Cu(II)_5(L_3)_4(NO_3)_2]\cdot 3H_2O$ ***(6)***

$Cu(NO_3)_2.3H_2O$ (0.25 g, 1.034 mmol), 2-(methylamino)phenyl hydroxamic acid (L_3H_2) (0.17 g, 1.035 mmol) and NaOH (0.041 g, 1.025 mmol) were dissolved in methanol (25 cm^3) and stirred at room temperature for 4 h. The resultant dark green solution was subsequently filtered and X-ray quality crystals of **6** were obtained upon slow evaporation after one week in a 44% yield. Elemental analysis (%) calculated as $[Cu(II)_5(L_3)_4(NO_3)_2]$ ($C_{32}H_{32}N_{10}O_{14}Cu_5$): C 34.99, H 2.94, N 12.75. Found: C 35.31, H 3.20, N 12.99. FT-IR (cm^{-1}): 3430 (w), 3135 (m) 2925 (m), 1635 (m), 1593 (s), 1551 (s), 1467 (m), 1383 (s), 1160 (m), 1137 (m), 1091 (s), 1039 (s), 937 (m), 777 (m), 753 (m), 689 (s), 653 (s).

$[Cu(II)_5(L_4H)_4(MeOH)_2(NO_3)_2]\cdot 3H_2O\cdot 4MeOH$ (7).

$Cu(NO_3)_2.3H_2O$ (0.25 g, 1.04 mmol), *N*-hydroxy-2-((2-hydroxy-3-methoxybenzyl)amino benzamide (L_4H_3) (0.38 g, 1.04 mmol) and NaOH (0.042 g, 1.04 mmol) were dissolved in MeOH (30 cm^3) and stirred for 4 hrs at room temperature. The resultant dark green solution was then filtered and X-ray quality crystals of **7** were obtained upon slow evaporation of the mother liquor in 20% yield. Elemental analysis (%) calculated as $[Cu(II)_5(L_3H)_4(H_2O)_2(NO_3)_2]\cdot 7H_2O$ ($C_{60}H_{74}N_{10}O_{31}Cu_5$): C 41.20, H 4.27, N 8.01. Found: C 40.91, H 4.07, N 7.86. FT-IR (cm^{-1}): 3375 (br), 3071 (w), 2938 (m), 2839 (m), 1907 (w), 1732 (m), 1611 (s, sh), 1592 (w), 1515 (w), 1482 (s, sh), 1442 (m), 1371 (m), 1328 (m), 1272 (s), 1163 (m), 1083 (s), 1058 (m), 986 (m), 913 (w), 829 (w), 747 (s), 687 (m), 538 (m).

Notes and references

‡ Footnotes relating to the main text should appear here. These might include comments relevant to but not central to the matter under discussion, limited experimental and spectral data, and crystallographic data.

References

1. (a) D. Griffith, M. Devocelle and C. J. Marmion. Hydroxamic Acids: Their Chemistry, Bioactivity, Solution and Solid Phase Synthesis in Amino Acids, Peptides and Proteins in Organic Chemistry, ed. A. B. Hughes, 2009, vol. 2, pp. 93; (b) M. Paris, M. Porcelloni, M. Binaschi and D. Fattori, *J. Med. Chem.*, 2008, **51**, 1505; (c) R. Codd, *Coord. Chem. Rev*., 2008, **252**, 1387; (d) Z. Amtul, R. Attaur, R. A. Siddiqui and M. I. Choudhary, *Curr. Med. Chem.*, 2002, **9**, 1323; (e) D. T. Puerta and S. M. Cohen, Curr. *Top. Med. Chem*., 2004, **4**, 1551.

2. (a) E. M. F. Muri, M. J. Nieto, R. D. Sindelar and J. S. Williamson, *Curr. Med. Chem.*, 2002, **9**, 1631; (b) C. J. Marmion, D. Griffith and K. B. Nolan, *Eur. J. Inorg. Chem*., 2004, 3003.

3. B. Kurzak, H. Kozlowski and E. Farkas. *Coord. Chem. Rev.*, 1992, **114**, 169.

4. (a) D. S. Kalinowski, D. R. Richardson. *Pharmacol. Rev.*, 2005, **57(4)**, 547. (b) M. R. Bedford, S. J. Ford, R. D. Horniblow and C. Tselepis. *J. Clin. Pharmacol.*, 2013, **53**, 885.

5. (a) K.N. Raymond, E.A. Dertz, in: J.H. Crosa, A.R. Mey, S.M. Payne (Eds.), Iron Transport in Bacteria, ASM Press, Washington, DC, 2004, p. 3. (b) A. Stintzi, K.N. Raymond, in: D.M. Templeton (Ed.), Molecular and Cellular Iron Transport, Marcel Dekker, Inc., New York, 2002, p. 273. (c) M. J. Miller, *Chem. Rev.*, 1989, **89**, 1563.

6. (a) A. M. Wilson, P. J. Bailey, P. A. Tasker, J. R. Turkington, R. A. Grant and J. B. Love, *Chem. Soc. Rev.*, 2014, **43**, 123; (b) B. K. Tait, K. E. Mdlalose and I. Taljaard, *Hydrometallurgy*, 1995, **38**, 1.

7. For an extensive review on metallacrowns see: (a) G. Mezei, C. M. Zaleski and V. L. Pecoraro, *Chem. Rev.*, 2007, **107**, 4933. (b) P. Happ, C. Plenk and E. Rentschler. *Coord. Chem. Rev.*, 2015, **289-290**, 238.

8. C. McDonald, S. Sanz, E. K. Brechin, M. K. Singh, G. Rajaraman, D. Gaynor, L. F. Jones. *RSC Advances*, 2014, **4**, 38182.

9. C. McDonald, T. Whyte, S. M. Taylor, S. Sanz, E. K. Brechin, D. Gaynor and L. F. Jones. *CrystEngComm,* 2013, **15**, 6672.

10. J. Comiskey, E. Farkas, K. A. Krot-Lacina, R. G. Pritchard, C. A. McAuliffe and K. B. Nolan, *Dalton. Trans.*, 2003, 4243.

11. Z. Eckstein, T. Jadach, and E. Lipczynska-Kochany, *J. Chem. Eng. Data*, 1983, **28**, 279.

12. E. Lipczynska-Kochany and H. Iwamura, *Chem. Lett.*, 1982, **11**, 1825.

13. G. Bonola and E. Sianesi, *J. Med. Chem.*, 1970, **13**, 329.

14. C. McDonald, D. W. Williams, P. Comar, S. J. Coles, T. D. Keene, M. B. Pitak, E. K. Brechin and L. F. Jones. *Dalton Trans*., 2015, **44**, 13359.

15. A. F. Abdel-Magid, K. G. Carson, B. D. Harris, C. A. Maryanoff and R. D. Shah. *J. Org. Chem.,* 1996, **61**, 3849.

16. (a) N. F. Chilton, R. P. Anderson, L. D. Turner, A. Soncini and K. S. Murray, *J. Comput. Chem.*, 2013, **34**, 1164. (b) O. Khan, *Molecular Magnetism*, VCH, New York, 1993.

17. (a) A. K. Powell, S. L. Heath, D. Gatteschi, L. Pardi, R. Sessoli, G. Spina, F. Del Giallo, F. Pieralli, *J. Am. Chem. Soc.*, 1995, **117**, 2491. (b) R. Werner, S. Ostrovsky, K. Griesar and W. Haase, *Inorg. Chim. Acta*, 2001, **326**, 78 (magnetostructural correlations Fe(III) dimers). (c) F. Le Gall, F. Fabrizi de Biani, A. Caneschi, P. Cinelli, A. Cornia, A. C. Fabretti and D. Gatteschi, *Inorg. Chim. Acta*, 1997, **262**, 123 (magnetostructural correlations on Fe(III) dimers). d) T. Weyhermüller, R. Wagner and P. Chaudhuri, *Eur. J. Inorg. Chem.*, 2011, 2547 (magnetostructural correlations on Fe(III) dimers).

18. (a) A. V. Pavlishchuk, S. V. Kolotilov, M. Zeller, L. K. Thompson, I. O. Fritsky, A. W. Addison and A. D. Hunter, *Eur. J. Inorg. Chem.*, 2010, 4851. (b) P. Happ, E. Rentschler, *Dalton Trans.*, 2014, **43**, 15308.

19. (a) A. A. Kitos, C. G. Efthymiou, C. Papatriantafyllopoulou, V. Nastopoulos, A. J. Tasiopoulos, M. J. Manos, W. Wernsdorfer, G. Christou and S. P. Perlepes, *Polyhedron*, 2011, **30**, 2987. (b) S.-H. Zhang, Y. Song, H. Liang, and M.-H. Zeng, *CrystEngComm*, 2009, **11**, 865. (c)V. Tudor, G. Marin, F. Lloret, V. Ch. Kravtsov, Y. A. Simonov, M. Julve and M. Andruh, *Inorg. Chim. Acta*, 2008, **361**, 3446. (d) S. T. Meally, C. McDonald, P. Kealy, S. M. Taylor, E. K. Brechin, *Dalton Trans.*, 2012, **41**, 5610. (e) A. Ferguson, A. Parkin, J. Sanchez-Benitez, K. Kamenev, W. Wernsdorfer, M. Murrie, *Chem. Commun.*, 2007, 3473.

20. Rigaku OD (2015). *CrysAlis PRO*. Rigaku Oxford Diffraction Ltd, Yarnton, England.

21. G. M. Sheldrick. *Acta Crystallogr. Sect. C Struct. Chem.,* 2015, **71**, 3.

22. A. L. Spek. *Acta Cryst. Sect. C.* 2015, **71**, 1-9.